Modelling of Density Changes of Nodular Cast Iron During Solidification by Cellular Automaton

D. Gurgul[1*], A. Burbelko[1], E. Guzik[1], D. Kopyciński and M. Królikowski[2]
[1]AGH University of Science and Technology, 23 Reymonta Str., 30-059 Krakow, Poland
[2]Odlewnie Polskie S.A., 70 Wyzwolenia Av., 27-200 Starachowice, Poland

Results of predictions of nodular cast iron density changes during solidification are presented. These changes were calculated by using a mathematical model which bases on a Cellular Automaton - Finite Differences (CA-FD) method. The CA-FD model takes into account, among others, the independent nucleation of graphite and austenite as a function of undercooling, the migration rate of the grains' borders, non-uniform distribution of temperature and concentration in the calculation domain, diffusion of the carbon in the liquid and the austenite. All simulation were performed at various: nucleation intensity and the eutectic saturation. It has been shown and proofed by other authors that the shrinkage phenomena take place at three stages: pre-eutectic shrinkage, eutectic expansion, and final shrinkage.

Keywords: cellular automaton, ductile iron, solidification modelling, density prediction.

Introduction

Nodular cast iron also known as ductile iron (DI) has major applications in critical engineering parts because of its mechanical and casting properties. These features of this material depend on the shape and number of graphite grains and on the structure of a metallic matrix. One of the most important thing in manufacture DI castings is the density changes during cooling and solidification.

Density of most materials increases during solidification. It means that the volume of the solid phase is smaller than the initial liquid phase. This causes in foundry engineering the need of use the feeding systems in order to eliminate the shrinkage defects. Exceptions to this rule, for example, water and bismuth are. Volume of these substances increases during the transformation from liquid state into solid state. It is caused by a specific structure of the crystal lattice. Similarly to water and bismuth the DI may behave under certain conditions. The reason for the volume expansion when cast iron solidifies (DI as well as grey cast iron – GCI) is precipitation of graphite which density is almost three times smaller than other phases. However, as the foundry practise shows, to obtain a "healthy" cast, with no shrinkage defects, made of DI is very difficult for small values of the casting's thermal module (under about 12 mm).[1]

The conditions at which graphite in DI grows are different from conditions of growth graphite in other kinds of cast iron. In GCI both primary and eutectic graphite are in permanent contact with the parent liquid phase. Additionally, the eutectic graphite grows with constant contact of three phases (graphite-austenite-liquid).

In DI the globules of the primary and the eutectic graphite, at initial stage, do not have a connection with austenite dendrites and they grow directly from the liquid.[2,3] Growing graphite particles deplete the liquid of the carbon. Such a poor carbon region is a privileged place for growing austenite. This results in acceleration of the austenite dendrite branches' growth in direction to graphite globules. After reaching the connection the austenite envelopes and isolates the graphite globules. Further growth of enclosed graphite nodules is also possible, because the carbon can diffuse from the liquid to the graphite surface through the austenite shell.

Analysed industrial castings, made of DI in one of the Polish foundry, are characterised by the same, known from literature, shrinkage defect typical for this alloy: [4]

1) the mechanism of feeders action is far more complicated than in alloys which have no expansion; sometimes elimination of feeders causes decrease of porosity,
2) minimal porosity level occurs in the eutectic alloys in which an increase of the carbon concentration in eutectic has a positive effect,
3) porosity of GCI casting is considerably smaller than in DI castings.

An example of shrinkage porosity that may occur in industrial castings made of DI is shown in Fig. 1. Such a defect has a negative effect on strength and leakproofness of castings.

* Corresponding author, email: dg@agh.edu.pl

a) b)

Fig. 1: An example of shrinkage defect in a DI casting (a); a place of the section indicated by the arrow (b).

Another examples of shrinkage defects (shrinkage cavities in feeders) in DI castings made of EN-GJS-400-18 are presented in Fig. 2. Carbon concentration was evaluated by use of Active Carbon Equivalent (ACE) which was measured by Adaptive Thermal Analysis System (ATAS). The value of ACE changed from 4.15 to 4.28 wt.%. Fig. 2 shows that the higher carbon concentration is the smaller volume of voids in the feeders is. Unfortunately, experience dictates that it does not always lead to the reduction of the level of shrinkage defects.

a) b) c) d)

Fig. 2: Influence of the ACE on the cavity shape in feeders for DI EN-GJS-400-18; ACEL values: a) 4.15 wt.%, b) 4.18 wt.%, c) 4.22 wt.%, d) 4.28 wt.%.

The mechanism of shrinkage defect formation is still under discussion, even though it is obvious that the main reason for this is the volume change of alloy during cooling and phase transformation. This paper presents assessments of the specific volume change in DI during solidification by use of the CA-FD.

The CA-FD model

Models which adopt a cellular automaton technique and the finite different method are one of the known methods used in computer modelling of solidification. They have been a subject of many studies.[5-15] All of these models are used for mono-phase transformations. Models used for two-phase solidification are also known,[3,16] but they are not as numerous as single-phase.

The CA-FD model used in this paper can calculate the microstructure of DI for binary Fe-C system during cooling of a casting at a superimposed cooling rate. The model takes into account: the continuous nucleation of austenite and graphite grains, separate non-equilibrium growth of the graphite nodules and the austenite dendrites at the initial stage of solidification, and cooperative growth of the graphite-austenite eutectic at further stage. In order to do this it is required to take into consideration, in the computational model, a number of physical phenomena such as: heat flow, carbon diffusion, interfacial energy and its influence on the crystallization front, heterogeneous nucleation, and release of latent heat.

The distinctive features of the CA-FD models is fact that the inner structure and the shape of growing grains are not superimposed at the beginning of calculations. They are effect of conditions which occur at the crystallization front during solidification. In order to obtain the satisfactory inner structure and the shape of grains (both for austenite dendrites and graphite nodules) the calculation meshes used for temperature and concentration fields should have the spatial step equal to the order of one micrometre. Such a small step limits using this method only for micro regions in two-dimensional space. It is caused by limited memory and computational power of modern computers.

The kinetic undercooling is a measure of the thermodynamic driving force of phase transformation. The total undercooling at the interface is equal to the difference between the equilibrium temperature T_{eq} (as a function of carbon

content) and the real temperature T_r at the front. On the other hand this difference is equal to the sum of the capillary undercooling ΔT_κ and the kinetic undercooling ΔT_μ:

$$T_{eq} - T_r = \Delta T_\kappa + \Delta T_\mu \tag{1}$$

where $\Delta T\kappa = \Gamma \cdot \kappa$, Γ is the Gibbs-Thomson coefficient, and κ is the front curvature.

The interface migration rate was assumed as a linear function[17] of the local kinetic undercooling ΔT_μ:

$$u = \mu \Delta T_\mu \tag{2}$$

where μ is the kinetic growth coefficient (various for austenite and graphite).

The heat flow in the computational domain was described by the Fourier equation:

$$c\frac{\partial T}{\partial \tau} = \nabla(\lambda \nabla T) + q_T + q_{cool} \tag{3}$$

where: T is the temperature, τ is the time, λ is the thermal conductivity, c is the volumetric specific heat. The terms q_T and q_{cool} are the source of latent heat generation rate and the intensity of external cooling respectively.

The carbon diffusion in the domain is similarly described to equation (3) by the following equation:

$$\frac{\partial C}{\partial \tau} = \nabla(D \nabla T) + q_C \tag{4}$$

where D is the carbon diffusion coefficient (various for liquid and austenite), and C is the carbon concentration in the appropriate phase. The term q_c is responsible for the carbon rejection by the crystallization front. This is caused by different solubility of the carbon in the liquid and the austenite.

Both equations (3) and (4) were numerically solved by using the finite differences (FD) method.

Grain nucleation in industrial alloys has a heterogeneous nature. Substrates for nuclei are randomly distributed in the bulk. The size of the substrates also has a stochastic nature. The undercooling at which a substrate becomes active is a function of substrates' size. The functional relationship between the active substrate fraction and the undercooling ΔT should be expressed by a probability distribution law.[18] The undercooling value of each phase should be calculated relatively to the appropriate liquidus line. The number n of active substrates in a domain V at undercooling ΔT below the equilibrium temperature can be calculated on the basis of a cumulative distribution function $F(\Delta T)$:

$$n = N_{\max} F(\Delta T) V \tag{5}$$

where $N_{\max}$ is the maximum specific number of substrates for nucleation.

In the CA-FD model as function $F(\Delta T)$ the Weibull cumulative distribution was assumed:[19]

$$F(\Delta T) = \exp(-b/\Delta T) \tag{6}$$

where b is an experimental coefficient.

Only one substrate is placed in the small domain V (a cell of the CA) if the n value is greater than the random number p generated with the equiprobability distribution in the (0..1] range. The undercooling of the potential nucleation in this case is estimated as an inverse function of the equation (6):

$$\Delta T = -b/\ln(p/(N_{\max} V)) \tag{7}$$

More details of stochastic nucleation are described in.[20]

The cellular automaton (CA) adopted to this model has a set of six states of cells. At the beginning of simulation all cells have the same state – liquid. When the temperature inside a cell drops down below the equilibrium temperature this cell may change its state from liquid to transitional state. The transitional state means that inside this cell a phase transformation can happen. There are three types of the transitional states: the transition from liquid into austenite $L \rightarrow \gamma$, from liquid to graphite $L \rightarrow gr$, and, when a graphite nodule grows inside austenite, the transition from austenite to graphite $\gamma \rightarrow gr$. An increment Δf of a new phase inside each transitional cell is calculated by the fallowing equation:

$$\Delta f = \frac{u \Delta \tau}{a(|\cos\theta| + |\sin\theta|)} \tag{8}$$

where: $\Delta\tau$ is the time step, a is the side length of the CA cell (for square cells), and θ the angle between the X axis and the normal direction to the front.

When a transitional cell finishes the transformation it changes its state into a solid state. There are two types of solid states. If the transformation $L \rightarrow gr$ or $\gamma \rightarrow gr$ takes place, the cell gets the graphite state. For the transformation $L \rightarrow \gamma$ the cell is changed into the austenite state.

Other details of the CA-FD model are introduced elsewhere.[21-24]

Density estimation

Density of specific phases was determined by means of CALPHAD method,[25] using Thermo-CALC® software. Obtained from Thermo-CALC® data were used for creating regression equations. For each phase the density changes ρ, kg/m^3, as a function of temperature (for liquid, austenite and graphite) and carbon concentration (only for liquid and austenite) were determined. The equations have the following forms:

– for the liquid phase:

$$\rho_L = 8192.2 - 0.5402 \cdot T - 9805.3 \cdot C \tag{9}$$

– for the austenite phase:

$$\rho_\gamma = 8238.7 - 0.48684 \cdot T - 3876.0 \cdot C - 5982.0 \cdot C^2 \tag{10}$$

– for the graphite phase:

$$\rho_{gr} = 2292.9 - 0.067442 \cdot T \tag{11}$$

where: T is temperature, K; C is carbon mass fraction.

The equations (9), (10) and (11) work in temperature range from 1010 K to 1610 K. The concentration ranges for equations (9) and (10) are from 3.9 to 4.8 mass % and from 0.5 to 2.5 mass % respectively.

Simulation results

The calculations were performed for a modelling alloy that solidifies like DI (with divorced eutectic). All simulations were conducted on a computational mesh with 640×640 cells and a spatial step equal to 2 μm. The thermophysical properties of the modelling alloy are listed in Table 1. The are adequate to the binary Fe-C alloy. Three variants of chemical composition were analysed: eutectic (C_0=4.25 wt.% C), hypoeutectic ($0.95 \cdot C_0$), and hypereutectic ($1.05 \cdot C_0$).

Samples were cooled with a cooling rate which is typical for a DI casting with 9 mm wall thickness moulded in a greensand mould:

$$q_{cool} = -5.082 \cdot c_v \cdot \exp\left(-5.307 \cdot 10^3 \cdot \tau\right) \tag{12}$$

where c_v is the mean volumetric specific heat for the alloy.

In the simulations it made an analysis for the alloy with various intensity of nucleation. In the calculations it was analysed the influence of a number of graphite spheroids on the alloy density change during solidification. A graphite nodules number depends on an amount of inoculant which is put into the alloy during so-called secondary metallurgy or out-of-furnace alloy treatment. In the simulations the change of the nucleation intensity was considered by a various number of the coefficient N_{max}: 10^9, 10^{10} and 10^{11} m^{-2}.

The obtained cooling curves presented in Fig. 3. As it can be noticed the increase of the nodule number does not impact practically on the duration process. The increase of the nodule number causes the fact that the transformation requires lower undercooling and it takes place at higher temperatures. The maximal recalescence is observed in DI samples with hypereutectic composition. In samples with hypoeutectic composition the recalescence does not appear practically.

Density changes for DI together with changes of liquid fraction are presented in Fig. 4. In this figure it is shown that independently of the eutectic level the density changes can be divided into three stages: pre-eutectic shrinkage, eutectic expansion, and final shrinkage. The presence of the pre-eutectic shrinkage, both in eutectic and slightly hypereutectic DI, has been proved by an experiment[26] carried out by using Combined Liquid Displacement and Cooling Curve Analysis (CLD CCA) method. In contrast, the final shrinkage in DI with hypoeutectic composition has been experimentally proved in. [27]

The pre-eutectic shrinkage also takes place in hypereutectic DI. The precipitation of the primary graphite slows down slightly the shrinkage at this stage of solidification, but it does not eliminate the shrinkage completely. The better a sample is inoculated, the inhibition of the shrinkage begins earlier. In this case, the transition into the eutectic expansion also happens earlier. The reason of the pre-eutectic shrinkage in hypereutectic DI is decreasing of the liquid density when the temperature of the alloy drops down. The partial expansion of DI, caused by the primary graphite solidification, only decreases the intensity of the pre-eutectic shrinkage. However, this expansion does not compensate completely for the shrinkage.

The minimal density values, at the instant when the eutectic expansion finishes and when the final shrinkage starts, are listed in the Table 2 (the numerators). The increase of the graphite nodules number results in the small density decrease. The amount of the vanishing liquid in this moment is shown in the Table 2 as the denominators. In DI with a smaller number of graphite nodules the final shrinkage begins earlier, when the liquid volume fraction is grater and equal to about 5 %.

Table 1: The thermophysical properties used in the modelling.

Heat conductivity ($W \cdot m^{-1} \cdot K^{-1}$):		
– liquid[9]	λ_L	30
– austenite[28]	λ_γ	20
– graphite[9]	λ_{gr}	20
Diffusivity of carbon in (m^2/s):		
– liquid[29]	D_L	$1.25 \cdot 10^{-9}$
– austenite[9]	D_γ	$5 \cdot 10^{-10}$
Latent heat (J/m^3):		
– liquid – austenite[30]	$L_{L\to\gamma}$	$19.7 \cdot 10^{8}$
– liquid – graphite	$L_{L\to gr}$	$16.2 \cdot 10^{5}$
– austenite – graphite	$L_{\gamma\to gr}$	$8.8 \cdot 10^{5}$
Specific heat ($J \cdot m^{-3} \cdot K^{-1}$):		
– liquid[30]	c_L	$5.6 \cdot 10^{6}$
– austenite[9]	c_γ	$5.84 \cdot 10^{6}$
– graphite[30]	c_{gr}	$1.78 \cdot 10^{6}$
Gibbs-Thomson coefficient for interface ($m \cdot K$):		
– austenite – liquid[30]	$\Gamma_{L\to\gamma}$	$1.9 \cdot 10^{-7}$
– graphite – liquid	$\Gamma_{L\to gr}$	$7.0 \cdot 10^{-6}$
– graphite – austenite	$\Gamma_{\gamma\to gr}$	$9.45 \cdot 10^{-6}$
Kinetic coefficient of the interface ($m \cdot s^{-1} \cdot K^{-1}$):		
– austenite – liquid[31]	$\mu_{\gamma/L}$	10^{-3}
– graphite – liquid	$\mu_{gr/L}$	10^{-8}
– graphite – austenite	$\mu_{gr/\gamma}$	10^{-8}

The presented density, in the Table 2 and in the Fig 4, does not take into account potential shrinkage porosity. The real density can be lower which is caused by presence of discontinuity in material.

Table 2: The ratio between the minimal alloy density and the liquid fraction at the moment when the final shrinkage begins.

Alloy Composition	Graphite nucleation coefficient N_{max}, m^{-2}		
	10^9	10^{10}	10^{11}
Hypoeutectic	6959.6/5.51	6948.4/2.15	6942.0/1.60
Eutectic	6923.2/5.45	6910.7/2.17	6905.2/1.35
Hypereutectic	6884.8/4.34	6873.5/2.41	6868.0/1.20

As it follows from Table 2 and Fig. 4, better inoculation (higher N_{max}) results in the decreasing of the residual liquid phase volume at the instant of eutectic expansion termination and final shrinkage start.

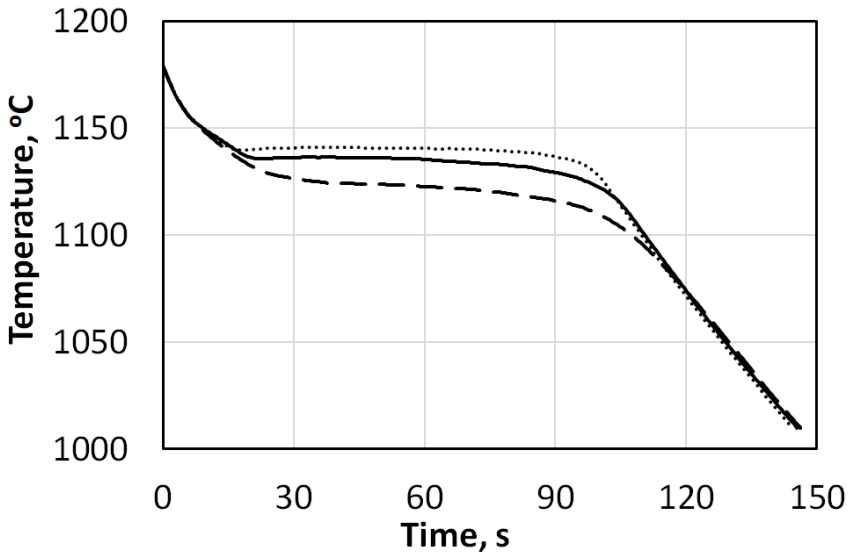

a)

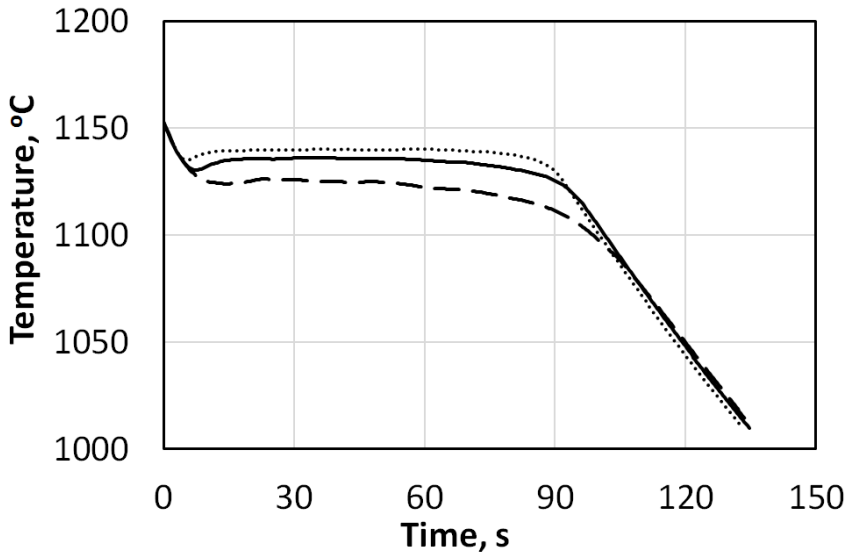

b)

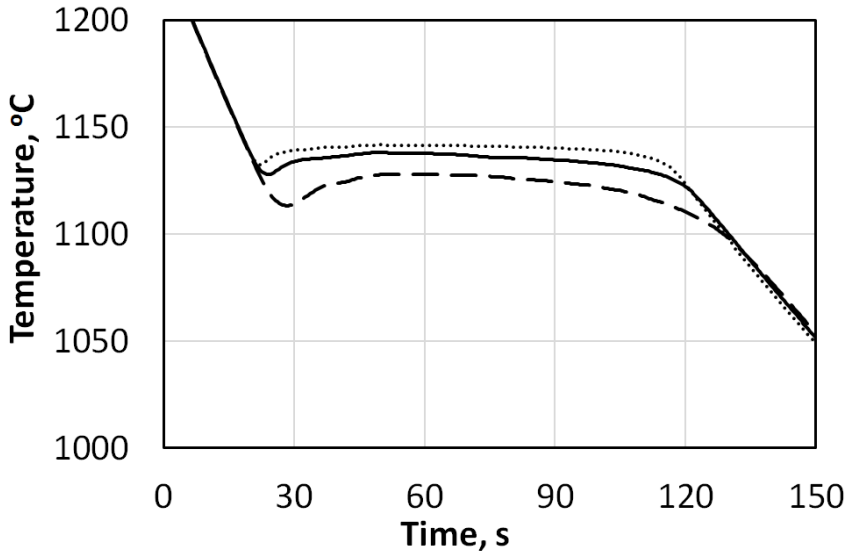

c)

Fig. 3: Cooling curves of the analysed alloys for the graphite nucleation coefficient N_{max}: 10^9, m^{-2} – the dashed lines, 10^{10}, m^{-2} – the solid lines, 10^{11}, m^{-2} –the dotted lines; a) the hypoeutectic alloy, b) the eutectic alloy, c) the hypereutectic alloy.

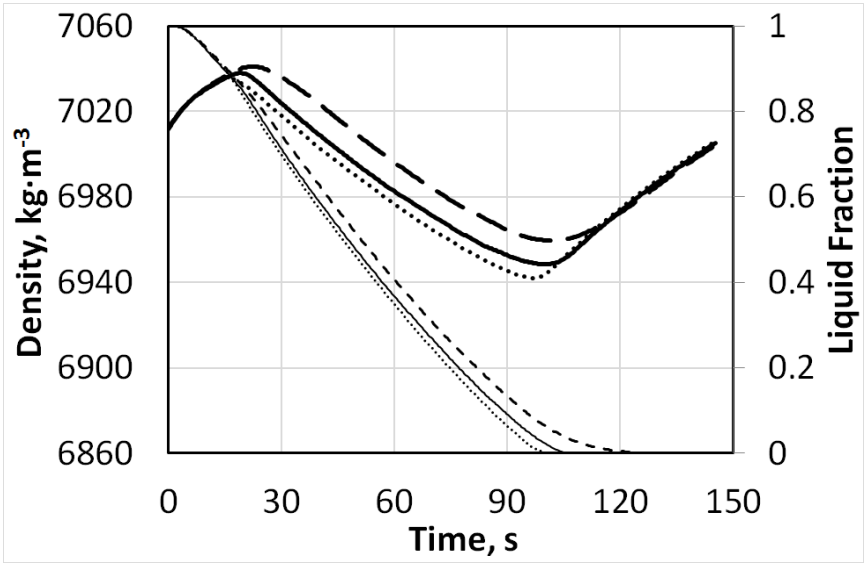

a)

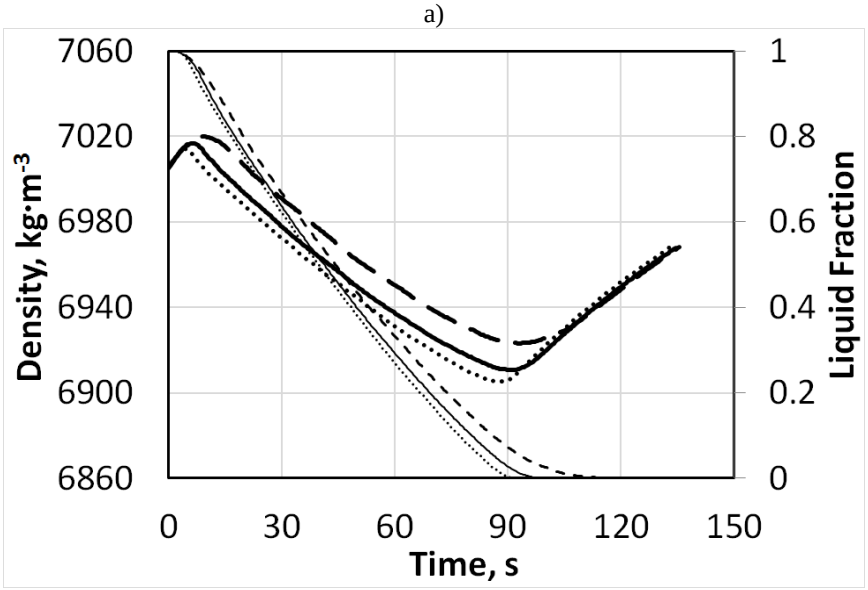

b)

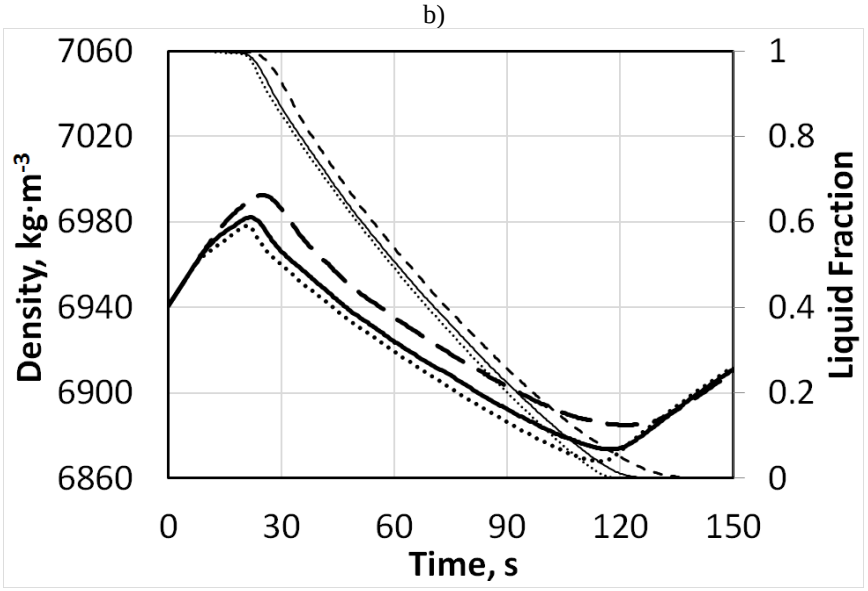

c)

Fig. 4: The density changes of DI (bold lines) and the liquid fraction (thin lines) during solidification; the graphite nucleation coefficient N_{max}: 10^9, m^{-2} – dashed lines, 10^{10}, m^{-2} – solid lines, 10^{11}, m^{-2} – dotted lines; a) hypoeutectic alloy, b) eutectic alloy, c) hypereutectic alloy.

Conclusions

1. In the paper a new tool has been tested which was designed to confirm by calculation the variability of the density of DI cast iron resulting from the additivity of precipitated phases.
2. It has been confirmed by numerical calculations that the density changes for hypoeutectic, eutectic, and hypereutectic alloys proceeds at three stages: the pre-eutectic shrinkage, the eutectic expansion, and the final shrinkage.
3. The pre-eutectic shrinkage in the DI occurs not only in the hypoeutectic or eutectic alloy. In the hypereutectic alloys it is caused by the fact that the effect of the expansion, which is generated by the primary graphite solidification, is weaker than the effect of the simultaneous liquid density increasing during the temperature dropping.
4. The observed density changes are consistent with the results obtained by use of the CLD CCA method.[26, 27]

References

1. The Sorelmetal Book of Ductile Iron. Rio Tinto Iron & Titanium, 174, 2004.
2. H. Fredriksson, J. Stjerndahl and J. Tinoco: *Mater. Sci. Eng., A*, 2005, 413-414, 363-372.
3. A. Burbelko, E. Fraś, D. Gurgul and J. Sikora: *Key Eng. Mater.*, 2011, 457, 330-336.
4. I. Ohnaka, A.Sato, A. Sugiyama and F. Kinoshita: *Int. J. Cast Met. Res*., 2008, 21, 11-16.
5. A.R. Umantsev, V.V. Vinogradov and V.T. Borisov: *Kristallografia*, 1985, 30, 455-460.
6. M. Rappaz and Ch.A. Gandin: *Acta Met. et Materialia*, 1993, 41, 345-360.
7. S. Pan and M. Zhu: *Acta Mater*., 2010, 58, 340-352.
8. G. Guillemot, Ch.A. Gandin, M. Bellet: *J. Cryst. Growth*, 2007, 303, 58-68.
9. L. Beltran-Sanchez and D.M. Stefanescu: *Metall. Mat. Trans. A*, 2004, 35, 2471-2485.
10. V. Pavlyk and U. Dilthey: *Model. Simul. Mat. Sci. Eng*., 2004, 12, 33-45.
11. M.F. Zhu and C.P. Hong: *ISIJ Int*., 2002, 42, 520-526.
12. D.S. Svyetlichnyy: *Comput. Mater. Sci*., 2012, 60, 153-162.
13. A.A. Burbelko, E. Fraś, W. Kapturkiewicz and D. Gurgul: *Mat. Sci. Forum*, 2010, 649, 217-222.
14. D.J. Jarvis, S.G.R. Brown and J.A. Spittle: *Mat. Sci. Techn*., 2000, 16, 1420-1424.
15. A.A. Burbelko, E. Fraś, W. Kapturkiewicz and E. Olejnik: *Mat. Sci. Forum*, 2006, 508, 405-410.
16. H.L. Zhao, M.F. Zhu and D.M. Stefanescu: *Key Eng. Mater.*, 2011, 457, 324-329.
17. J. Hoyt and M. Asta: *Phys. Rev. B.*, 2002, 65, 1-11.
18. Ch.A. Gandin and M. Rappaz: *Acta Metall. Mater*., 1994, 42, 2233-2246.
19. E. Fraś, K. Wiencek, M. Górny and H. Lopez: *Archives of Metallurgy*, 2001, 46, 317-333.
20. W. Kapturkiewicz, A.A. Burbelko, E. Fraś, M. Górny and D. Gurgul: *Journal of Achievements in Materials and Manufacturing Engineering*, 2010, 43, 310-323.
21. A. Burbelko, D. Gurgul, W. Kapturkiewicz and M. Górny: *Mat. Sci. Eng.*, 2012, 33, 012083, 1-9.
22. A.A. Burbelko, D. Gurgul, W. Kapturkiewicz and M. Górny: *Archives of Foundry Engineering*, 2012, 12, 11-16.
23. A. Burbelko and D. Gurgul: *Computer Methods in Materials Science*, 2011, 11, 128-134.
24. D. Gurgul and A. Burbelko: *Archives of Metallurgy and Materials*, 2010, 55, 53-60.
25. H.L. Lukas, S.G. Fries and B. Sundman: 'Computational Thermodynamics: The Calphad Method', University Press, Cambridge, 2007.
26. D.M. Stefanescu, M. Moran, S. Boonmee, and W.L. Guesser: *AFS Proceedings 2012*, American Foundry Society, Schaumbur, IL. USA, 2012, Paper 12-045, 1-9.
27. G. Alonso, D.M. Stefanescu, R. Suarez, A. Loizaga, and G. Zarrabeitia: *Int. J. Cast Met. Res.*, 2014, 27, 87-100.
28. I.K. Kikoin, ed., 'Tables of the physical parameters', 1976, Moskow, Avtomizdat, (in Russian).
29. P. Magnin, J.T. Mason and R. Trivedi; *Acta Met. et Mater.*, 1991, 39, 469-480.
30. B. Chopard and M. Droz: 'Cellular Automata Modeling of Physical Systems', 2005, Cambridge University Press.
31. A. Burbelko: 'Modeling of solidification process by cellular automata method', 2004, Krakow, UWND AGH, (in Polish).

Acknowledgement

The study was co-financed by NCBiR in the years 2012-2015 as a targeted project No. INNOTECH/IN1/13/150421/NCBR/12